Translational Oncology
www.transonc.com

Volume 6 Number 5 October 2013 pp. 607–617 607

The Microenvironment of Cervical Carcinoma Xenografts: Associations with Lymph Node Metastasis and Its Assessment by DCE-MRI[1]

Christine Ellingsen*, Stefan Walenta†, Tord Hompland*, Wolfgang Mueller-Klieser† and Einar K. Rofstad*

*Department of Radiation Biology, Institute for Cancer Research, Oslo University Hospital, Oslo, Norway; †Institute of Physiology and Pathophysiology, University Medical Center of the Johannes Gutenberg University of Mainz, Mainz, Germany

Abstract

Poor disease-free and overall survival rates in locally advanced cervical cancer are associated with a tumor microenvironment characterized by extensive hypoxia, interstitial hypertension, and high lactate concentrations. The potential of gadolinium diethylenetriamine pentaacetic acid–based dynamic contrast-enhanced magnetic resonance imaging (DCE-MRI) in assessing the microenvironment and microenvironment-associated aggressiveness of cervical carcinomas was investigated in this preclinical study. CK-160 and TS-415 cervical carcinoma xenografts were used as tumor models. DCE-MRI was carried out at 1.5 T, and parametric images of K^{trans} and v_e were produced by pharmacokinetic analysis of the DCE-MRI series. Pimonidazole was used as a marker of hypoxia. A Millar catheter was used to measure tumor interstitial fluid pressure (IFP). The concentrations of glucose, adenosine triphosphate (ATP), and lactate were measured by induced metabolic bioluminescence imaging. High incidence of lymph node metastases was associated with high hypoxic fraction and high lactate concentration in CK-160 tumors and with high IFP and high lactate concentration in TS-415 tumors. Low K^{trans} was associated with high hypoxic fraction, low glucose concentration, and high lactate concentration in tumors of both lines and with high incidence of metastases in CK-160 tumors. Associations between v_e and microenvironmental parameters or metastatic propensity were not detected in any of the tumor lines. Taken together, this preclinical study suggests that K^{trans} is a potentially useful biomarker for poor outcome of treatment in advanced cervical carcinoma. The possibility that K^{trans} may be used to identify patients with cervical cancer who are likely to benefit from particularly aggressive treatment merits thorough clinical investigations.

Translational Oncology (2013) 6, 607–617

Introduction

Locally advanced squamous cell carcinoma of the uterine cervix is treated with radiation alone or radiation in combination with chemotherapy and/or surgery. The recommended treatment in the western world is concurrent cisplatin-based chemotherapy and radiation therapy [1,2]. The overall survival after concurrent radiochemotherapy is ~70%, which is ~10% higher than that after radiation therapy alone [3]. The addition of chemotherapy to radiation therapy causes increased side effects, particularly hematological and gastrointestinal toxicities [3]. Novel biomarkers that can predict the outcome of radiation therapy of locally advanced cervical cancer are highly warranted for establishing procedures for personalized treatment [3,4].

The most important tumor-related prognostic factors in cervical cancer are tumor size, stage, cell type, and lymph node involvement [4]. Cervical carcinomas develop an abnormal physiological microenvironment during growth characterized by hypoxia, interstitial hypertension, high lactate concentrations, low glucose concentrations, and energy deprivation [5,6]. During the last decade, it has become

Address all correspondence to: Einar K. Rofstad, PhD, Department of Radiation Biology, Institute for Cancer Research, Oslo University Hospital, Box 4953 Nydalen, N-0424 Oslo, Norway. E-mail: einar.k.rofstad@rr-research.no

[1]The authors thank the Norwegian Cancer Society, the South-Eastern Norway Regional Health Authority, the Deutsche Forschungsgemeinschaft (MU576/15-1 and 15-2), and the German Federal Ministry of Education and Research ("ISIMEP," 02NUK016A) for financial support.
Received 26 March 2013; Revised 24 June 2013; Accepted 8 July 2013

DOI 10.1593/tlo.13313

increasingly clear that the prognostic and predictive value of these abnormalities may be significant. Thus, extensive hypoxia in the primary tumor has been shown to be associated with locoregional treatment failure and poor disease-free and overall survival rates in patients with advanced disease [7–10], and studies of patients with cervical cancer treated with radiation therapy alone have shown that high interstitial fluid pressure (IFP) in the primary tumor is linked to high probability of pelvic recurrence and distant metastases [11–13]. Moreover, the disease-free and overall survival rates have been shown to be particularly poor for patients with cervical cancer with high lactate concentrations in the primary tumor [14,15]. Interestingly, Fyles et al. [12] have measured both IFP and oxygen tension in the primary tumor of more than 100 patients with advanced cervical carcinoma, and this study showed no correlation between either IFP or hypoxic fraction and established tumor-related prognostic factors.

Useful biomarkers for personalized treatment of locally advanced cervical cancer should most likely reflect the physiological microenvironment of the tumor tissue [4]. There is significant evidence from preclinical studies that dynamic contrast-enhanced magnetic resonance imaging (DCE-MRI) with gadolinium diethylenetriamine pentaacetic acid (Gd-DTPA) as contrast agent may have the potential to provide microenvironment-associated tumor biomarkers [16]. A DCE-MRI–based method is particularly attractive in patients with cervical cancer, because DCE-MRI is an established and commonly used method for anatomic characterization of the tumor tissue in these patients. Initial investigations of the prognostic value of DCE-MRI in cervical cancer have provided interesting results [17,18]. Significant correlations have been found between DCE-MRI–derived parameters and local tumor control, disease-free survival, and/or overall survival [19–23]. Highly different protocols were used for image acquisition and analysis in these investigations, and consequently, comparisons of observations are difficult. However, apparently conflicting results have been reported. In some studies, DCE-MRI parameters reflecting high angiogenic activity and blood perfusion were found to be indicative of poor prognosis [20,21], whereas poor prognosis was reported to be associated with DCE-MRI parameters reflecting poor vascularization and hypoxia in other studies [22,23]. Few clinical investigations have compared DCE-MRI parameters with parameters of the physiological tumor microenvironment of cervical carcinomas [24–26]. Significant correlations have been found between DCE-MRI–derived parameters and hypoxia-associated parameters of the tumor tissue, including microvascular density and oxygen tension [25,26]. However, the correlations are weak, perhaps because the DCE-MRI was carried out under suboptimal conditions or because of inadequate analysis of the DCE-MRI series.

In preclinical studies, DCE-MRI can be carried out under well-controlled conditions, and the physiological microenvironment of imaged tumors can be assessed in great detail. Experimental tumors should therefore be useful for investigating whether DCE-MRI may provide biomarkers for microenvironment-associated poor prognosis in cancer. The potential of DCE-MRI–derived parametric images as biomarkers for tumor aggressiveness in cervical cancer was investigated in the present study by using CK-160 and TS-415 cervical carcinoma xenografts as preclinical models of human disease. The CK-160 and TS-415 xenograft lines were selected for the study, because individual tumors of these lines show highly different physiological microenvironments and differ significantly in metastatic propensity [27]. To search for associations between metastatic propensity and characteristics of the tumor microenvironment and to investigate whether DCE-MRI–derived parameters may reflect the microenvironment, tumors were subjected to DCE-MRI and measurement of IFP before the host mice were killed and the tumors were resected. The mice were examined for metastatic growth, and the resected tumors were subjected to immunohistochemical assessment of fraction of hypoxic tissue and assessment of the concentrations of glucose, ATP, and lactate by induced metabolic bioluminescence imaging (imBI).

Materials and Methods

Tumor Models

CK-160 and TS-415 human cervical carcinoma xenografts growing in adult female BALB/c *nu*/*nu* mice were used as tumor models [27]. Tumors were initiated from cells cultured in RPMI 1640 (25 mM Hepes and L-glutamine) medium supplemented with 13% bovine calf serum, 250 mg/l penicillin, and 50 mg/l streptomycin. Approximately 5.0×10^5 cells in 10 μl of Hanks' balanced salt solution were inoculated in the gastrocnemius muscle. Tumors with volumes of 400 to 600 mm^3 were included in the study. DCE-MRI and IFP measurements were carried out with mice anesthetized with fentanyl citrate (0.63 mg/kg), fluanisone (20 mg/kg), and midazolam (10 mg/kg). Animal care and experimental procedures were in accordance with the Interdisciplinary Principles and Guidelines for the Use of Animals in Research, Marketing, and Education (New York Academy of Sciences, New York, NY).

Dynamic Contrast-Enhanced Magnetic Resonance Imaging

DCE-MRI was carried out as described earlier [28,29]. Briefly, Gd-DTPA (Schering, Berlin, Germany) was administered in a bolus dose of 0.3 mmol/kg. T_1-weighted images [repetition time (TR) = 200 ms, echo time (TE) = 3.2 ms, and α_{T1} = 80°] were recorded at a spatial resolution of $0.23 \times 0.23 \times 2.0$ mm^3 and a time resolution of 14 seconds by using a 1.5-T whole-body scanner (Signa; General Electric, Milwaukee, WI) and a slotted tube resonator transceiver coil constructed for mice. The coil was insulated with styrofoam to prevent excessive heat loss from the mice. The body core temperature of the mice was kept at 37 to 38°C during imaging by using a thermostatically regulated heating pad. Two calibration tubes, one with 0.5 mM Gd-DTPA in 0.9% saline and the other with 0.9% saline only, were placed adjacent to the mice in the coil. The tumors were imaged axially in a single section through the tumor center by using an image matrix of 256×128, a field of view of 6×3 cm^2, and one excitation. Two proton density images (TR = 900 ms, TE = 3.2 ms, and α_{PD} = 20°) and three T_1-weighted images were acquired before Gd-DTPA was administered, and T_1-weighted images were recorded for 15 minutes after the administration of Gd-DTPA. Gd-DTPA concentrations were calculated from signal intensities by using the method of Hittmair et al. [30]. The DCE-MRI series were analyzed on a voxel-by-voxel basis by using the arterial input function of Benjaminsen et al. [31] and the Tofts pharmacokinetic model [32]. According to this model,

$$C_t(T) = \frac{K^{trans}}{(1 - Hct)} \cdot \int_0^T C_a(t) \cdot e^{(-K^{trans} \cdot (T-t)/v_e)} dt,$$

where $C_t(T)$ is the concentration of contrast agent in the tissue at time T, $C_a(T)$ is the arterial input function, Hct is the hematocrit, K^{trans} is the volume transfer constant of the contrast agent, and v_e is the fractional distribution volume of the contrast agent in the tissue

[32]. Parametric images of K^{trans} and v_e were generated from the best curve fits to plots of C_t *versus* T by using the SigmaPlot software. Our algorithms produced unphysiological v_e values for voxels consisting primarily of necrotic tissue. Necrotic tissue regions were omitted in the analysis by excluding voxels with $v_e < 0.1$ and $v_e > 0.8$. Median values were calculated for the viable tissue of each tumor and used as parameters for the K^{trans} and v_e of individual tumors. Strengths and limitations of our DCE-MRI method have been discussed elsewhere [28,29].

Assessment of IFP

IFP was measured in the tumor center with a Millar SPC 320 catheter equipped with a 2F Mikro-Tip transducer (Millar Instruments, Houston, TX) [33]. The catheter was connected to a computer through a Millar TC-510 control unit and a preamplifier. Data acquisition was carried out by using the LabVIEW software (National Instruments, Austin, TX).

Immunohistochemical Assessment of Fraction of Hypoxic Tissue

1-[(2-Hydroxy-3-piperidinyl)-propyl]-2-nitroimidazole (pimonidazole) was used as a marker of tumor hypoxia [34]. The tumors were fixed in phosphate-buffered 4% paraformaldehyde, and histologic sections were prepared by using standard procedures. Immunohistochemistry was performed by using an avidin-biotin-peroxidase–based staining method [35]. An anti-pimonidazole rabbit polyclonal antibody (gift from Professor Raleigh, Department of Radiation Oncology, University of North Carolina School of Medicine, Chapel Hill, NC) was used as primary antibody. Diaminobenzidine was used as chromogen, and hematoxylin was used for counterstaining. Three cross sections were examined for each tumor. The area fraction of the tissue staining positive for pimonidazole was determined by image analysis and was used as a parameter for hypoxic fraction [34].

imBI of Glucose, ATP, and Lactate Levels

Glucose, ATP, and lactate concentrations were measured in serial tumor cryosections by the imBI method, as described earlier [36–38]. Briefly, reaction solutions containing specific enzymes linking the metabolite of interest to the luciferase of *Photobacterium fischeri* or *Photinus pyralis* were used. Light emission was induced in a temperature-stabilized reaction chamber positioned on the stage of a microscope (Axiophot; Zeiss, Oberkochen, Germany) connected to a 16-bit electron-multiplying charge-coupled device (EM-CCD) camera with an imaging photon counting system (iXonEM + DU-888; Andor Technology PLC, Belfast, United Kingdom). Images of the spatial distribution of light intensities were calibrated by using appropriate standards. Metabolite concentrations were acquired exclusively from histologically viable tissue by interactive optical microdissection. The concentrations were calculated in micromoles per gram of tumor tissue and were displayed in color-coded images. Three sections per metabolite were analyzed for each tumor, and the mean value was used as a parameter for the metabolite concentration of a tumor. Further methodological details and representative calibration curves have been reported elsewhere [15,39].

Assessment of Metastatic Status

Spontaneous metastasis was studied as described elsewhere [27]. Briefly, tumor-bearing mice were killed and examined for external lymph node metastases in the inguinal, axillary, interscapular, and submandibular regions and internal lymph node metastases in the abdomen and mediastinum. The presence of metastatic growth in enlarged lymph nodes was confirmed by histologic examinations.

Statistical Analysis

Curves were fitted to data by linear regression analysis. Correlations between variables were searched for by using the Pearson product moment correlation test. Statistical comparisons of data were carried out by using the Student's t test when the data complied with the conditions of normality and equal variance. Under other conditions, comparisons were carried out by nonparametric analysis using the Mann-Whitney rank sum test. The Kolmogorov-Smirnov method was used to test for normality. Multivariate logistic regression analysis was used to identify parameters predictive of metastasis. Probability values (P) and correlation coefficients (R^2) were calculated by using the SigmaStat statistical software. A significance criterion of $P < .05$ was used.

Results

Eighteen CK-160 and 16 TS-415 tumors were included in the study. The intratumor heterogeneity in glucose, ATP, and lactate concentration was significant in both tumor lines. This is illustrated in Figure 1, which shows the glucose, ATP, and lactate images of a representative CK-160 tumor (Figure 1*A*) and a representative TS-415 tumor (Figure 1*B*). Furthermore, the glucose, ATP, and lactate concentrations differed substantially among the individual tumors of each line. This is also illustrated in Figure 1, which shows plots of glucose concentration *versus* ATP concentration, glucose concentration *versus* lactate concentration, and ATP concentration *versus* lactate concentration for the 18 CK-160 tumors (Figure 1*C*) and the 16 TS-415 tumors (Figure 1*D*). In the CK-160 line, there was a positive correlation between the concentrations of glucose and ATP ($P = .0010$), an inverse correlation between the concentrations of glucose and lactate ($P = .0058$), and no correlation between the concentrations of ATP and lactate ($P > .05$). However, there was no correlation between these metabolic parameters in the TS-415 line.

The tumors of both lines showed highly heterogeneous staining for pimonidazole (Figure 2*A*). The staining patterns were consistent with staining of hypoxic cells without staining of normoxic cells. Positive staining of cells adjacent to blood vessels could not be detected in any of the lines. Necrotic regions were always encompassed by a rim of pimonidazole-positive cells, a feature that was particularly pronounced in the TS-415 tumors, which showed a histologic appearance characterized by bands of viable tissue surrounding relatively large necroses. Foci of pimonidazole-positive cells scattered throughout the tissue were seen in tumor regions without necrosis. These foci differed substantially in size and shape, and a few necrotic or necrotizing cells could be observed in the middle of some of the foci. Staining intensity gradients were seen in some CK-160 tumors, whereas the boundary line between stained and unstained cells was sharp in most TS-415 tumors.

Fraction of hypoxic tissue (HF_{Pim}) differed from 23% to 53% among the 18 CK-160 tumors and from 8% to 39% among the 16 TS-415 tumors. The intertumor heterogeneity in IFP was also significant. IFP differed from 2.5 to 31.2 mm Hg (CK-160) and from 11.3 to 64.5 mm Hg (TS-415). None of the lines showed a significant correlation between HF_{Pim} and IFP (data not shown).

There was a positive correlation between HF_{Pim} and lactate concentration ($P = .0078$), an inverse correlation between HF_{Pim} and

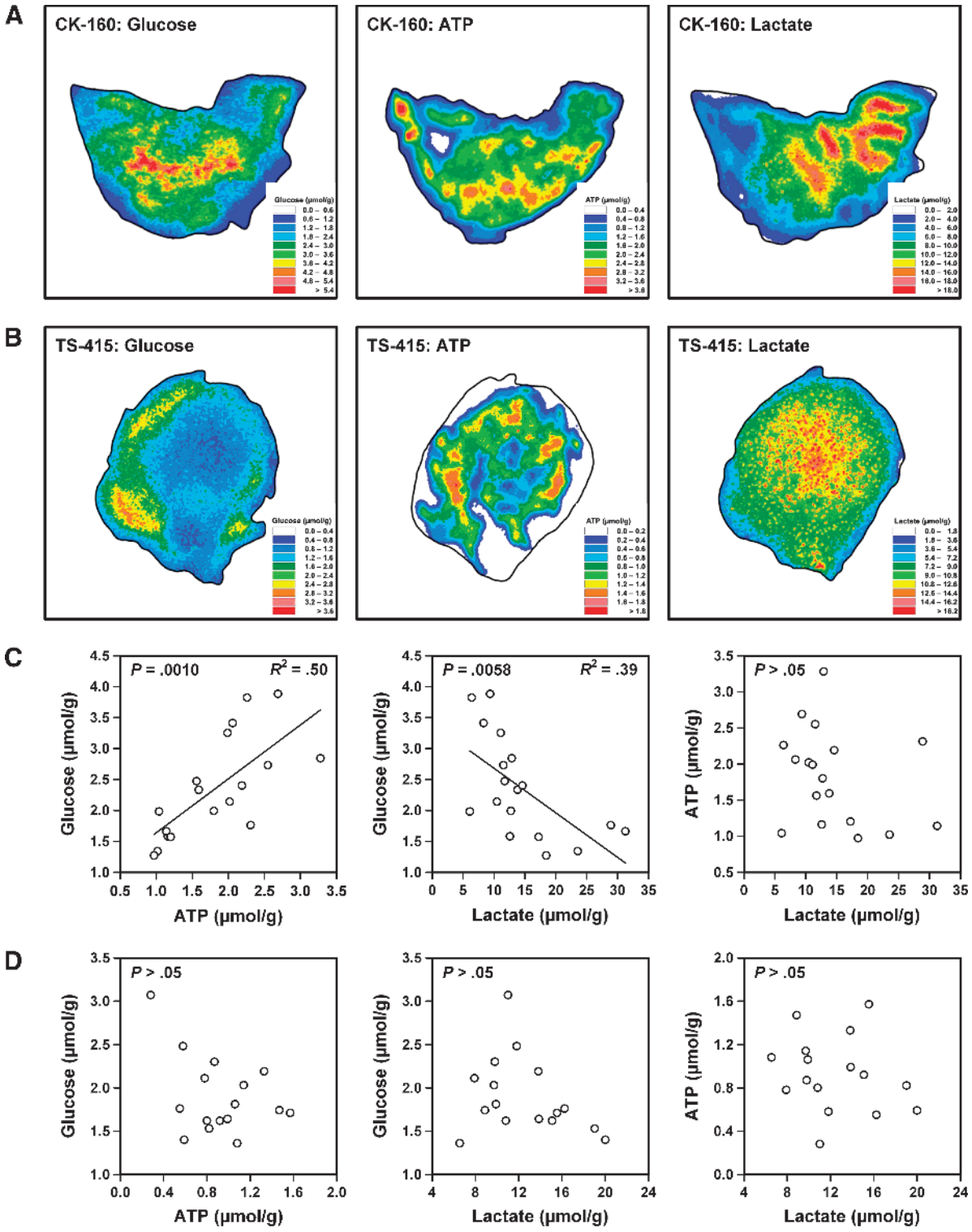

Figure 1. Glucose, ATP, and lactate concentration images of a representative CK-160 tumor (A) and a representative TS-415 tumor (B) as measured by imBI and plots of glucose concentration *versus* ATP concentration, glucose concentration *versus* lactate concentration, and ATP concentration *versus* lactate concentration for CK-160 (C) and TS-415 (D) tumors. Points represent single tumors. Curves were fitted to data by linear regression analysis.

glucose concentration ($P = .030$), and no correlation between HF_{Pim} and ATP concentration ($P > .05$) in the CK-160 tumors (Figure 2*B*). Similarly, the TS-415 tumors showed a positive correlation between HF_{Pim} and lactate concentration ($P = .0041$), a trend toward an inverse correlation between HF_{Pim} and glucose concentration ($P = .084$), and no correlation between HF_{Pim} and ATP concentration ($P > .05$; Figure 2*C*). There was no correlation between IFP and these metabolic parameters in any of the lines (data not shown).

Lymph node metastases were detected in 9 of the 18 mice bearing CK-160 tumors and in 9 of the 16 mice bearing TS-415 tumors, whereas the other mice were metastasis-negative. In the CK-160 line, the metastatic tumors showed higher HF_{Pim} ($P = .00028$) and higher lactate concentration ($P = .016$) than the nonmetastatic tumors but did not differ from the nonmetastatic tumors in IFP ($P > .05$), glucose concentration ($P > .05$), and ATP concentration ($P > .05$; Figure 3*A*). In the TS-415 line, the metastatic tumors showed higher IFP ($P = .011$) and higher lactate concentration ($P = .017$) than the nonmetastatic tumors but did not differ from the nonmetastatic tumors in HF_{Pim} ($P > .05$), glucose concentration ($P > .05$), and ATP concentration ($P > .05$; Figure 3*B*). Multivariate statistical analysis showed that only HF_{Pim} was predictive of metastasis in CK-160 tumors ($P < .001$) and that IFP and lactate concentration were independent predictors of metastasis in TS-415 tumors ($P < .05$).

Representative DCE-MRI data are presented in Figure 4, which shows the K^{trans} image, K^{trans} frequency distribution, v_e image, and v_e frequency distribution of a CK-160 tumor with a relatively low HF_{Pim} of 28% (Figure 4*A*), a TS-415 tumor with a relatively low HF_{Pim} of 16% (Figure 4*B*), a CK-160 tumor with a relatively high HF_{Pim} of 50% (Figure 4*C*), and a TS-415 tumor with a relatively high HF_{Pim} of 39% (Figure 4*D*). The tumors of both lines were highly heterogeneous in K^{trans} with the highest values in the periphery and the lowest values in central regions. The intratumor heterogeneity in v_e was also substantial but did not follow a fixed pattern in any of the lines (i.e., low and high values were seen in the center as well as in the periphery of the tumors). Furthermore, both tumor lines showed substantial intertumor heterogeneity in K^{trans} and v_e, but a significant correlation between K^{trans} and v_e was not seen in any of the lines (data not shown).

Figure 5 shows plots of K^{trans} *versus* HF_{Pim} and the concentrations of lactate and glucose for the 18 CK-160 tumors (Figure 5*A*) and the 16 TS-415 tumors (Figure 5*B*). In both lines, there was an inverse correlation between K^{trans} and HF_{Pim} [$P = .000061$ (CK-160); $P = .000093$ (TS-415)] and between K^{trans} and lactate concentration [$P = .00032$ (CK-160); $P = .0020$ (TS-415)] and a positive correlation between K^{trans} and glucose concentration [$P = .00055$ (CK-160); $P = .026$ (TS-415)]. However, K^{trans} did not correlate with IFP or ATP concentration in any of the lines, and furthermore, none of the lines showed a correlation between v_e and HF_{Pim}, IFP, or the concentration of lactate, glucose, or ATP (data not shown).

In the CK-160 line, K^{trans} was higher in the tumors of the metastasis-negative mice than in the tumors of the metastasis-positive mice

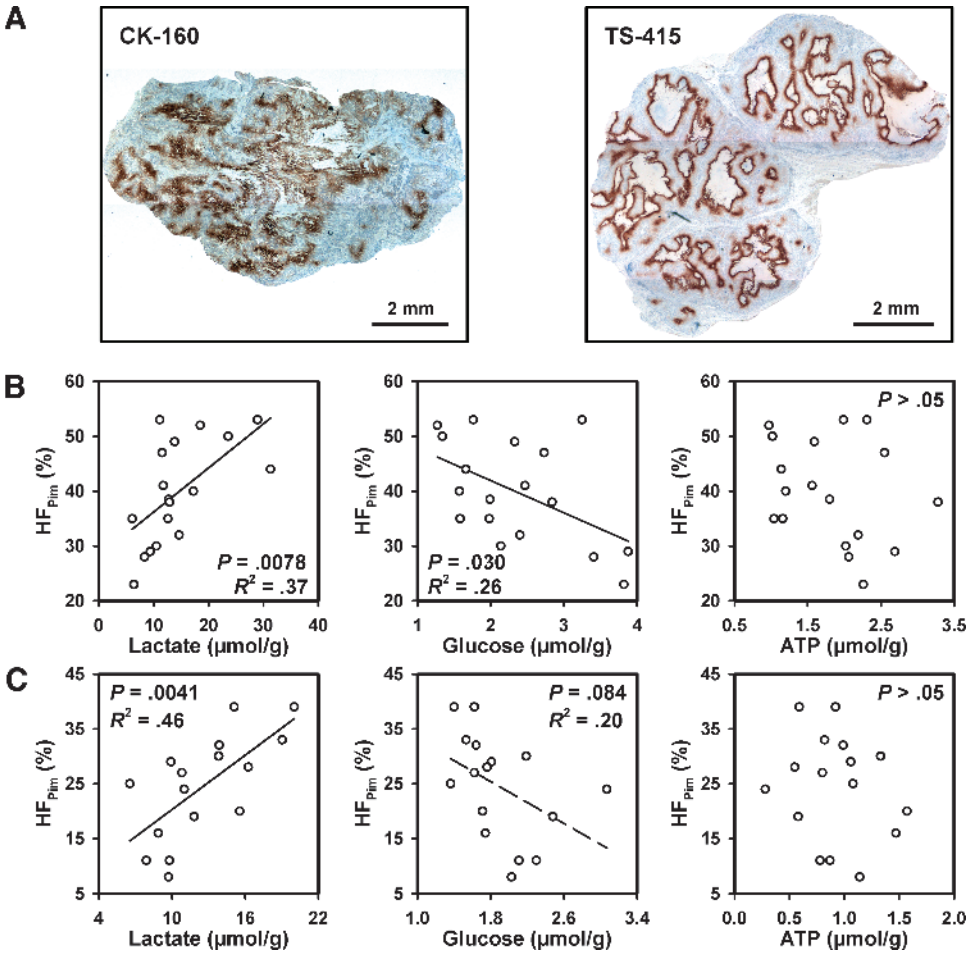

Figure 2. Representative immunohistochemical preparations of a CK-160 tumor and a TS-415 tumor stained with anti-pimonidazole antibody to visualize hypoxic tissue (A) and plots of HF_{Pim} *versus* lactate, glucose, and ATP concentrations for CK-160 (B) and TS-415 (C) tumors. Points represent single tumors. Curves were fitted to data by linear regression analysis.

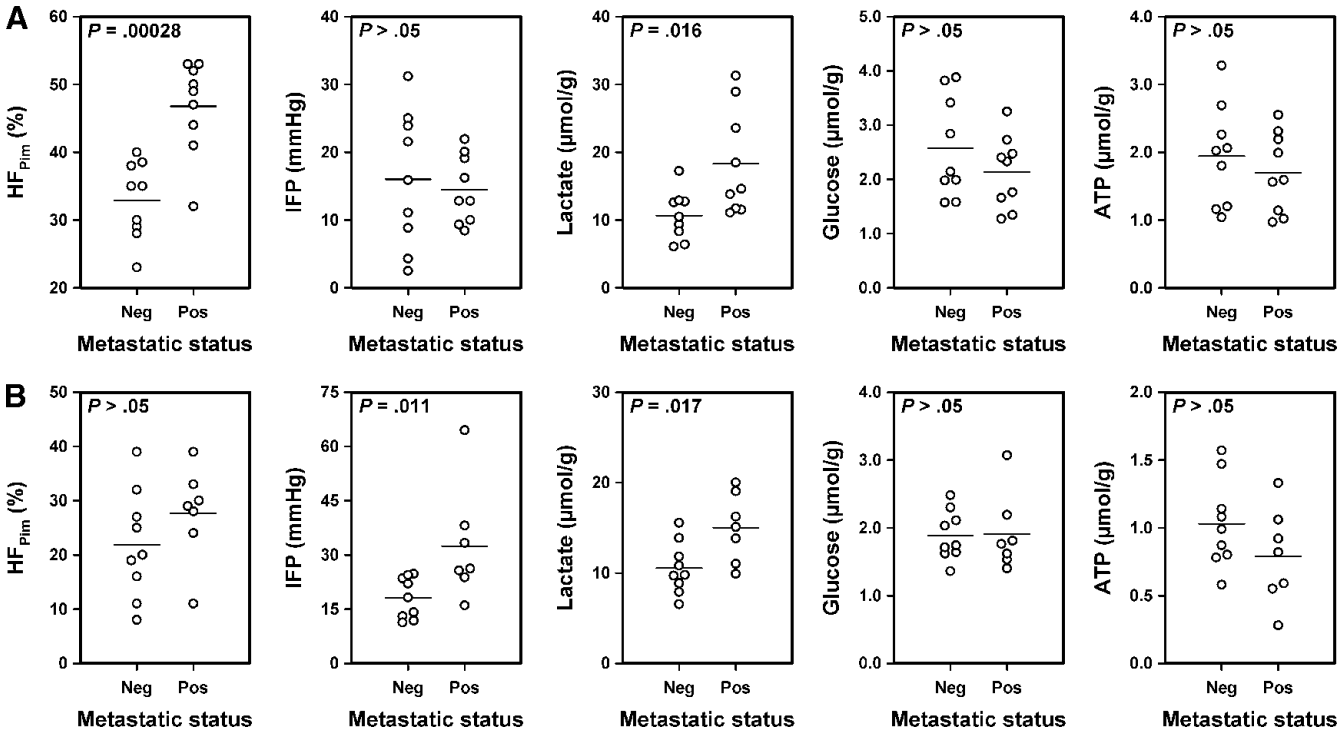

Figure 3. HF_{Pim}, IFP, and lactate, glucose, and ATP concentrations of nonmetastatic and metastatic CK-160 (A) and TS-415 (B) tumors. Points represent single tumors. Horizontal bars indicate mean values.

(P = .020), whereas v_e did not differ between nonmetastatic and metastatic tumors (P > .05; Figure 6*A*). In the TS-415 line, however, nonmetastatic and metastatic tumors did not differ in either K^{trans} (P > .05) or v_e (P > .05; Figure 6*B*).

Discussion

Methodological Considerations

The potential of DCE-MRI as a method for providing biomarkers for personalized treatment of cervical cancer cannot be evaluated properly without increased insight into the physiological microenvironment, associations between tumor aggressiveness and microenvironmental abnormalities, and associations between DCE-MRI–derived parameters and parameters of the tumor microenvironment. Eighteen CK-160 and 16 TS-415 tumors were included in this study, and K^{trans}, v_e, IFP, HF_{Pim}, metastatic status, and the concentrations of lactate, glucose, and ATP were measured in every single tumor. The strength of this experimental strategy is that it allows direct comparisons of data at the individual tumor level, thus avoiding potential misinterpretations associated with assessing different parameters in different tumor cohorts.

Tumor IFP was measured before tissue sections were prepared for assessment of HF_{Pim} and lactate, glucose, and ATP concentrations. The insertion of a Millar catheter into tumors is a rather invasive procedure, and signs of tissue destruction caused by the catheter were seen in some tissue sections. To avoid possible artifacts, tissue sections that were penetrated by the catheter were not used for assessment of HF_{Pim} or metabolite concentrations.

Tumor-bearing mice were scored as either metastasis-positive or metastasis-negative. A mouse was scored as metastasis-positive only when histologic examinations could confirm metastatic growth in at least one lymph node. Attempts to assess the number of positive lymph nodes were not made. The tumor transplantation site drained into the ipsilateral inguinal lymph nodes, and these lymph nodes constituted the principal site of metastatic growth. A mouse was scored as metastasis-negative when tumor growth could not be detected by histologic examination of these lymph nodes or any enlarged lymph node in other sites. This experimental procedure does not exclude the possibility that tiny metastatic deposits may have been overlooked and, hence, that metastasis-positive mice erroneously may have been scored as metastasis-negative.

Clinical investigations have shown that the intertumor heterogeneity of the physiological microenvironment is substantial in locally advanced cervical carcinoma. Fractions of hypoxic tissue varying from 8% to 95%, IFP values varying from −3 to 48 mm Hg, and lactate concentrations varying from 2.7 to 15.6 µmol/g have been reported [10,11,15]. Xenografted tumors of only two cervical carcinoma lines were included in the present work, which may be a limitation of our study. However, there are significant reasons to believe that results obtained with CK-160 and TS-415 tumors are transferable to the clinical setting. First, the physiological microenvironment differed substantially also among individual CK-160 and TS-415 tumors, most likely as a consequence of stochastic processes influencing initiation of angiogenesis shortly after tumor cell inoculation. Interestingly, the intertumor heterogeneity in hypoxic fraction, IFP, and lactate concentration in CK-160 and TS-415 tumors was comparable to that reported for cervical carcinomas in humans. Second, it has been shown that CK-160 and TS-415 xenografts retain essential biologic properties of the donor patients' tumors, including histologic appearance, radiation sensitivity, and metastatic pattern [27].

The Microenvironment of CK-160 and TS-415 Tumors

The energy metabolism of CK-160 tumors differed from that of TS-415 tumors. Glucose concentration was positively correlated to ATP concentration and inversely correlated to lactate concentration in CK-160 tumors but not in TS-415 tumors. It is possible that CK-160 tumors produce energy primarily from glucose, whereas TS-415 tumors also make significant use of other substrates such as glutamine [40,41]. Significant correlation between the concentrations of ATP and lactate was not seen in any of the lines, reflecting the general observation that cells tend to maintain a constant intracellular level of ATP during metabolic stress [41].

Tumor hypoxia is primarily a consequence of inadequate blood supply and increased oxygen consumption [42]. Interstitial hypertension in tumors is mainly a result of high geometric and viscous resistance to blood flow, low resistance to transcapillary fluid flow, and impaired lymphatic drainage [11]. Thus, tumor hypoxia and interstitial hypertension are partly consequences of microvascular abnormalities and partly consequences of vascular-unrelated abnormalities [41]. It has therefore been suggested that the fraction of hypoxic tissue and IFP may be closely related pathophysiological parameters in tumors. However, there was no correlation between HF_{Pim} and IFP in the present study, implying that these parameters are not governed by a common mechanism in CK-160 and TS-415 tumors. This observation is consistent with the clinical observation that tissue pO_2 is not correlated to IFP in cervical carcinoma [11].

As expected, IFP did not correlate with the concentration of lactate, glucose, or ATP in any of the tumor lines. In contrast, HF_{Pim} increased with increasing lactate concentration and decreased with increasing glucose concentration in both lines. However, the associations were weak, particularly the associations between hypoxia and glucose concentration. The concentration of glucose in tumor tissues is determined primarily by an equilibrium between the rate of glucose supply and the rate of glucose consumption, and similarly, the concentration of lactate is determined primarily by the rate of cellular production and the rate of clearance by the vasculature [41]. Tumor cells may produce lactate from glucose by aerobic as well as anaerobic glycolysis, and they generally show increased glucose consumption under hypoxic conditions [41,43]. The associations reported here

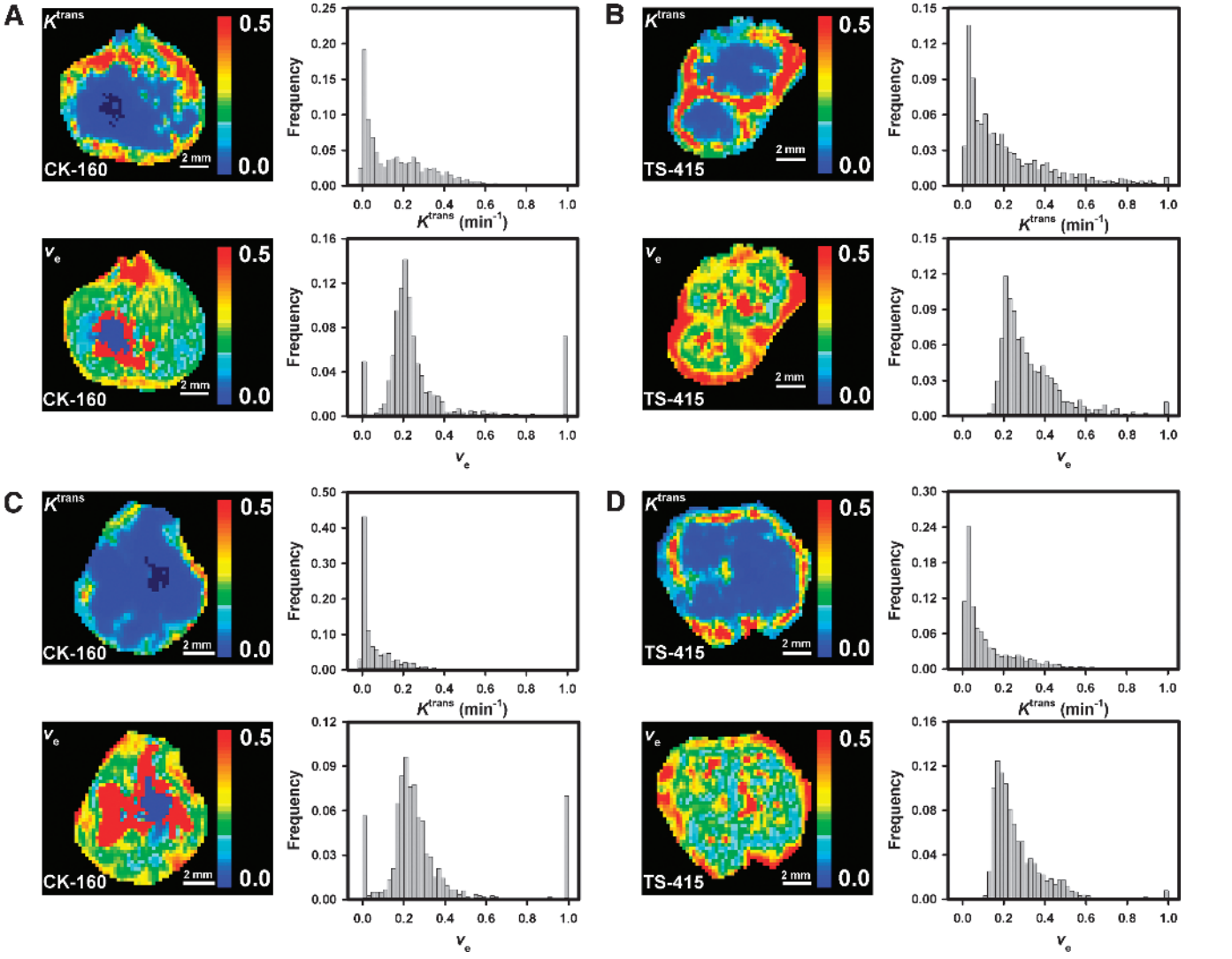

Figure 4. K^{trans} image, K^{trans} frequency distribution, v_e image, and v_e frequency distribution of a CK-160 tumor with a relatively low HF_{Pim} of 28% (A), a TS-415 tumor with a relatively low HF_{Pim} of 16% (B), a CK-160 tumor with a relatively high HF_{Pim} of 50% (C), and a TS-415 tumor with a relatively high HF_{Pim} of 39% (D).

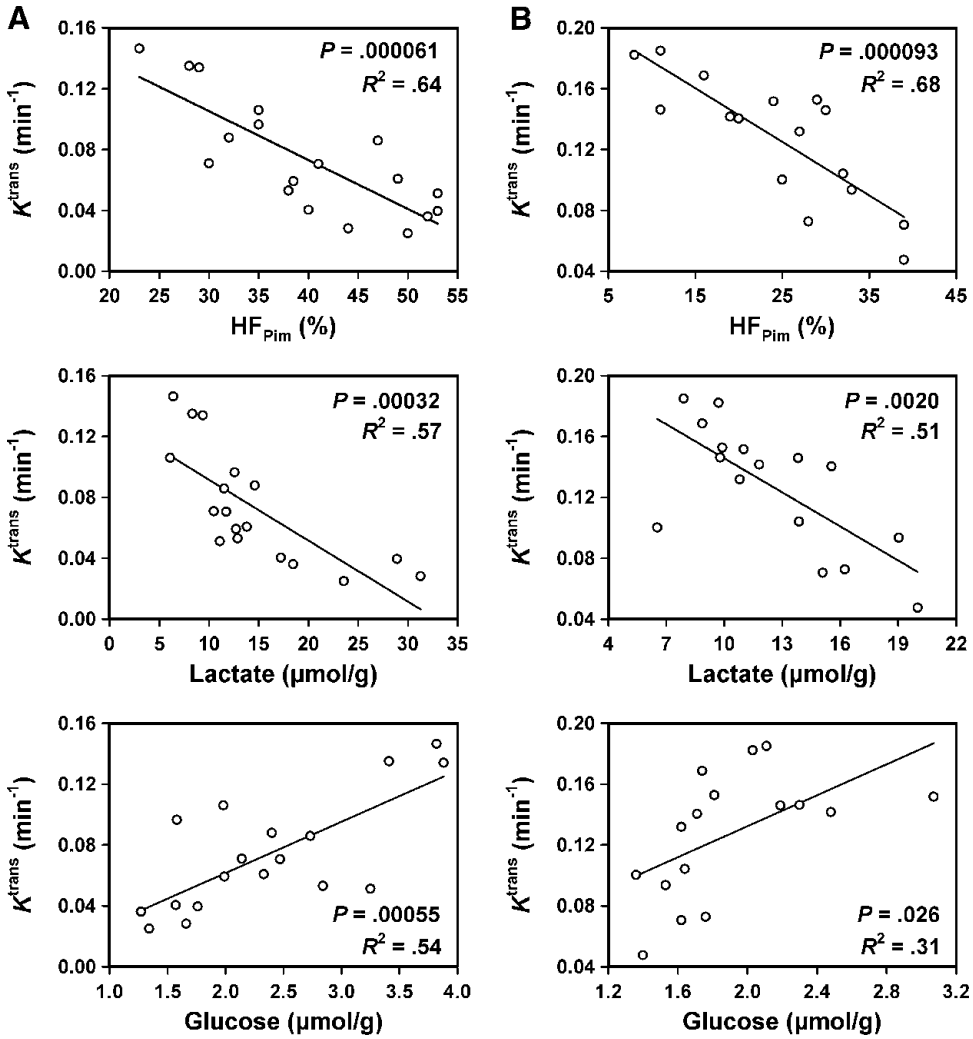

Figure 5. Plots of K^{trans} *versus* HF_{Pim} and the concentrations of lactate and glucose for CK-160 (A) and TS-415 (B) tumors. Points represent single tumors. Curves were fitted to data by linear regression analysis.

suggest that lactate is produced primarily by anaerobic glycolysis in CK-160 and TS-415 tumors, consistent with the observation that CK-160 and TS-415 cells in culture produce substantially more lactate under hypoxic than under aerobic conditions and the observation that CK-160 and TS-415 tumors primarily show chronic hypoxia as opposed to acute or cyclic hypoxia [44].

Associations between lactate concentration and hypoxic fraction have been searched for in several preclinical studies by comparing different tumor lines, individual tumors of the same line, and subregions of single tumors, and significant associations were found in some studies but not in others [45–48]. In general, the concentration of lactate is unrelated to the extent of hypoxia in tumors showing increased glycolytic flux [37,39,49]. For example, Yaromina et al. [48] studied xenografted tumors of three highly glycolytic cell lines derived from squamous cell carcinomas of the head and neck, observed that the average concentration of lactate did not correlate with the overall pimonidazole hypoxic fraction in any of the lines, and concluded that the extent of hypoxia cannot be predicted from the concentration of lactate. Busk et al. [50] assessed the relative partitioning between glycolytic and mitochondrial ATP synthesis in four squamous cell carcinoma cell lines, three of head and neck origin and one of cervical origin, and found that the ATP generation in all lines established from head and neck tumors relied on aerobic glycolysis, whereas the line established from a cervical tumor (SiHa) was found to show predominantly nonglycolytic ATP synthesis. The energy metabolism of CK-160 and TS-415 cervical carcinomas thus appears to be similar to that of SiHa cells and different from that of squamous cell carcinomas of the head and neck. Interestingly, it has been speculated that the glycolytic phenotype may be inherited from the tissue of tumor origin [50].

Microenvironment-Associated Metastasis in CK-160 and TS-415 Tumors

Clinical studies have shown that tumor aggressiveness is associated with severe abnormalities in the tumor microenvironment in cervical cancer [7–15]. The present preclinical investigation is consistent with this clinical observation and suggests that an abnormal microenvironment may promote lymph node metastasis in cervical carcinoma. Furthermore, our study suggests that different mechanisms may be involved in different tumors, depending on the nature of the abnormalities. High lactate concentration was associated with metastatic dissemination in both tumor lines, and in addition, development of metastases was associated with high HF_{Pim} in CK-160 tumors and with high IFP in TS-415 tumors. Noteworthy, lymph

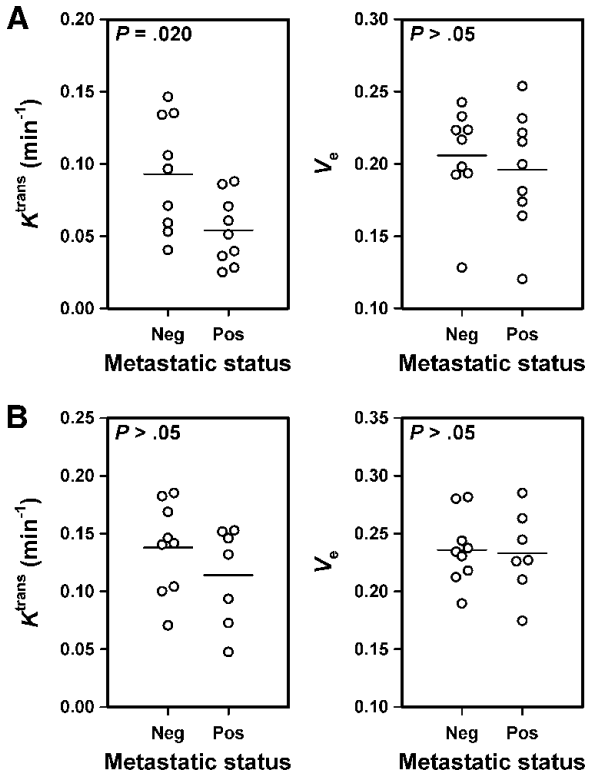

Figure 6. K^{trans} and v_e of nonmetastatic and metastatic CK-160 (A) and TS-415 (B) tumors. Points represent single tumors. Horizontal bars indicate mean values.

node metastasis was associated with high lactate concentration but not with high HF_{Pim} in TS-415 tumors, suggesting that the difference between metastatic and nonmetastatic tumors in lactate concentration was not merely a secondary consequence of a difference in extent of hypoxia.

Hypoxia may facilitate metastasis by inducing genomic instability, by selecting for aggressive cell phenotypes, and by upregulating the expression of metastasis-promoting genes [51,52]. Several transcription factors are activated by hypoxia including hypoxia-inducible factor-1 (HIF-1), and targets of HIF-1 play critical roles in many steps of the metastatic process, including cell viability/apoptosis, cell proliferation/growth arrest, tissue remodeling/invasion, tissue metabolism, and angiogenesis [53]. Elevated lactate levels may promote metastasis by hypoxia-dependent as well as hypoxia-independent mechanisms [49]. The hypoxia-independent mechanisms include lactate-induced stabilization of HIF-1α under normoxic conditions and lactate-induced activation of signaling pathways that promote cell migration and invasion [54]. High IFP directs interstitial fluid from tumors into the surrounding normal tissue, and this fluid carries proteolytic enzymes, chemokines, and lymphangiogenic factors that may facilitate lymph node metastasis by remodeling the extracellular matrix, dilating peritumoral lymphatics, and inducing lymphangiogenesis in the sentinel lymph node [55,56].

DCE-MRI in Assessment of the Aggressiveness of Cervical Carcinoma

The K^{trans} of both CK-160 and TS-415 tumors increased with increasing glucose concentration and decreased with increasing lactate concentration and increasing HF_{Pim}. Previous studies have revealed that HF_{Pim} is inversely correlated to the microvascular density of the viable tissue in CK-160 and TS-415 tumors and that the microvascular density is higher in TS-415 tumors than in CK-160 tumors [44,57]. Consequently, low values of K^{trans} were associated with a particularly hostile microenvironment in these tumors. Moreover, K^{trans} was lower in metastatic than in nonmetastatic CK-160 tumors, in accordance with the observation that the metastatic tumors showed higher HF_{Pim} and higher lactate concentration than the nonmetastatic tumors and the hypothesis that hypoxia and lactate may promote lymph node metastasis in cervical carcinoma. In contrast, K^{trans} did not differ significantly between metastatic and nonmetastatic TS-415 tumors, even though the metastatic tumors showed higher lactate concentration than the nonmetastatic tumors, possibly because high IFP exerted a stronger influence on the metastatic potential than did high lactate levels. This suggestion is consistent with the findings that IFP was higher in metastatic than in nonmetastatic TS-415 tumors and that there was no correlation between K^{trans} and IFP.

Several studies of cervical carcinoma have revealed weak but significant correlations between DCE-MRI–derived parameters and outcome of treatment. However, poor prognosis was associated with high signal enhancement in some studies and with low signal enhancement in others [20–23]. Poor correlations and conflicting results may reflect that the analyses were based on semiquantitative DCE-MRI parameters rather than quantitative parameters calculated by the use of pharmacokinetic models. For low-molecular-weight contrast agents like Gd-DTPA, low K^{trans} values indicate poor blood supply and are associated with low signal enhancement [32]. The present study thus suggests that low signal enhancement rather than high signal enhancement is indicative of poor prognosis in cervical carcinoma.

More importantly, the present study suggests that K^{trans} may be a significant predictive factor in cervical carcinoma. It can be hypothesized from our preclinical data that K^{trans} may discriminate well between tumors with severe and less severe microenvironmental abnormalities also in the clinical setting and, moreover, that K^{trans} may be developed to be a robust biomarker for tumor aggressiveness. This hypothesis deserves to be tested in comprehensive clinical investigations, and if found to be valid, it opens for the possibility that patients with low-K^{trans} tumors may be given highly aggressive concurrent radiochemotherapy, whereas patients with high-K^{trans} tumors may be spared for the side effects of aggressive treatment.

Even though K^{trans} may be useful for identifying particularly aggressive cervical carcinomas, pharmacokinetic analysis of DCE-MRI data is not sufficient to establish whether aggressiveness is primarily a consequence of extensive hypoxia, highly elevated IFP, or high lactate concentrations. To provide specific information on the physiological microenvironment of cervical carcinomas for targeted treatment strategies, supplementary MRI data are required. Particularly promising strategies include the use of blood oxygenation level–dependent MRI for assessment of tumor hypoxia [58], peritumoral fluid flow velocity DCE-MRI for assessment of IFP [59], and spectroscopic MRI for assessment of lactate levels [60].

In summary, low K^{trans} was associated with high hypoxic fraction, low glucose concentration, and high lactate concentration in human cervical carcinoma xenografts, and metastatic tumors showed high lactate concentrations in combination with either high hypoxic fractions or highly elevated IFP. These observations suggest that K^{trans} may be useful for characterizing the physiological microenvironment

of cervical carcinomas and, hence, a useful biomarker for microenvironment-induced tumor aggressiveness and treatment resistance. This possibility should be investigated thoroughly in prospective clinical studies.

References

[1] Barbera L and Thomas G (2009). Management of early and locally advanced cervical cancer. *Semin Oncol* **36**, 155–169.

[2] Al-Mansour Z and Verschraegen C (2010). Locally advanced cervical cancer: what is the standard of care? *Curr Opin Oncol* **22**, 503–512.

[3] Green J, Kirwan J, Tierney J, Vale C, Symonds P, Fresco L, Williams C, and Collingwood M (2005). Concomitant chemotherapy and radiation therapy for cancer of the uterine cervix. *Cochrane Database Syst Rev* **3**, CD002225.

[4] Klopp AH and Eifel PJ (2012). Biological predictors of cervical cancer response to radiation therapy. *Semin Radiat Oncol* **22**, 143–150.

[5] Höckel M and Vaupel P (2001). Biological consequences of tumor hypoxia. *Semin Oncol* **2**(suppl 8), 36–41.

[6] Vaupel PW and Kelleher DK (2012). Blood flow and associated pathophysiology of uterine cervix cancers: characterisation and relevance for localised hyperthermia. *Int J Hyperthermia* **28**, 518–527.

[7] Höckel M, Knoop C, Schlenger K, Vorndran B, Baussmann E, Mitze M, Knapstein PG, and Vaupel P (1993). Intratumoral pO_2 predicts survival in advanced cancer of the uterine cervix. *Radiother Oncol* **26**, 45–50.

[8] Höckel M, Schlenger K, Aral B, Mitze M, Schäffer U, and Vaupel P (1996). Association between tumor hypoxia and malignant progression in advanced cancer of the uterine cervix. *Cancer Res* **56**, 4509–4515.

[9] Fyles AW, Milosevic M, Wong R, Kavanagh MC, Pintilie M, Sun A, Chapman W, Levin W, Manchul L, Keane TJ, et al. (1998). Oxygenation predicts radiation response and survival in patients with cervix cancer. *Radiother Oncol* **48**, 149–156.

[10] Sundfør K, Lyng H, Tropé CG, and Rofstad EK (2000). Treatment outcome in advanced squamous cell carcinoma of the uterine cervix: relationships to pretreatment tumor oxygenation and vascularization. *Radiother Oncol* **54**, 101–107.

[11] Milosevic M, Fyles A, Hedley D, Pintilie M, Levin W, Manchul L, and Hill R (2001). Interstitial fluid pressure predicts survival in patients with cervix cancer independent of clinical prognostic factors and tumor oxygen measurements. *Cancer Res* **61**, 6400–6405.

[12] Fyles A, Milosevic M, Pintilie M, Syed A, Levin W, Manchul L, and Hill RP (2006). Long-term performance of interstitial fluid pressure and hypoxia as prognostic factors in cervix cancer. *Radiother Oncol* **80**, 132–137.

[13] Yeo SG, Kim JS, Cho MJ, Kim KH, and Kim JS (2009). Interstitial fluid pressure as a prognostic factor in cervical cancer following radiation therapy. *Clin Cancer Res* **15**, 6201–6207.

[14] Schwickert G, Walenta S, Sundfør K, Rofstad EK, and Mueller-Klieser W (1995). Correlation of high lactate levels in human cervical cancer with incidence of metastasis. *Cancer Res* **55**, 4757–4759.

[15] Walenta S, Wetterling M, Lehrke M, Schwickert G, Sundfør K, Rofstad EK, and Mueller-Klieser W (2000). High lactate levels predict likelihood of metastases, tumor recurrence, and restricted patient survival in human cervical cancers. *Cancer Res* **60**, 916–921.

[16] Gillies RJ, Raghunand N, Karczmar GS, and Bhujwalla ZM (2002). MRI of the tumor microenvironment. *J Magn Reson Imaging* **16**, 430–450.

[17] Hylton N (2006). Dynamic contrast-enhanced magnetic resonance imaging as an imaging biomarker. *J Clin Oncol* **24**, 3293–3298.

[18] Zahra MA, Hollingsworth KG, Sala E, Lomas DJ, and Tan LT (2007). Dynamic contrast-enhanced MRI as a predictor of tumour response to radiotherapy. *Lancet Oncol* **8**, 63–74.

[19] Yuh WTC, Mayr NA, Jarjoura D, Wu D, Grecula JC, Lo SS, Edwards SM, Magnotta VA, Sammet S, Zhang H, et al. (2009). Predicting control of primary tumor and survival by DCE MRI during early therapy in cervical cancer. *Invest Radiol* **44**, 343–350.

[20] Hawighorst H, Weikel W, Knapstein PG, Knopp MV, Zuna I, Schoenberg SO, Vaupel P, and van Kaick G (1998). Angiogenic activity of cervical carcinoma: assessment by functional magnetic resonance imaging-based parameters and a histomorphological approach in correlation with disease outcome. *Clin Cancer Res* **4**, 2305–2312.

[21] Donaldson SB, Buckley DL, O'Connor JP, Davidson SE, Carrington BM, Jones AP, and West CML (2010). Enhancing fraction measured using dynamic contrast-enhanced MRI predicts disease-free survival in patients with carcinoma of the cervix. *Br J Cancer* **102**, 23–26.

[22] Mayr NA, Wang JZ, Zhang D, Montebello JF, Grecula JC, Lo SS, Fowler JF, and Yuh WTC (2009). Synergistic effects of hemoglobin and tumor perfusion on tumor control and survival in cervical cancer. *Int J Radiat Oncol Biol Phys* **74**, 1513–1521.

[23] Andersen EKF, Hole KH, Lund KV, Sundfør K, Kristensen GB, Lyng H, and Malinen E (2012). Dynamic contrast-enhanced MRI of cervical cancers: temporal percentile screening of contrast enhancement identifies parameters for prediction of chemoradioresistance. *Int J Radiat Oncol Biol Phys* **82**, e485–e492.

[24] Lyng H, Vorren AO, Sundfør K, Taksdal I, Lien HH, Kaalhus O, and Rofstad EK (2001). Assessment of tumor oxygenation in human cervical carcinoma by use of dynamic Gd-DTPA-enhanced MR imaging. *J Magn Reson Imaging* **14**, 750–756.

[25] Hawighorst H, Knapstein PG, Weikel W, Knopp MV, Zuna I, Knof A, Brix G, Schaeffer U, Wilkens C, Schoenberg SO, et al. (1997). Angiogenesis of uterine cervical carcinoma: characterization by pharmacokinetic magnetic resonance parameters and histological microvessel density with correlation to lymphatic involvement. *Cancer Res* **57**, 4777–4786.

[26] Cooper RA, Carrington BM, Loncaster JA, Todd SM, Davidson SE, Logue JP, Luthra AD, Jones AP, Stratford I, Hunter RD, et al. (2000). Tumour oxygenation levels correlate with dynamic contrast-enhanced magnetic resonance imaging parameters in carcinoma of the cervix. *Radiother Oncol* **57**, 53–59.

[27] Ellingsen C, Natvig I, Gaustad JV, Gulliksrud K, Egeland TAM, and Rofstad EK (2009). Human cervical carcinoma xenograft models for studies of the physiological microenvironment of tumors. *J Cancer Res Clin Oncol* **135**, 1177–1184.

[28] Gulliksrud K, Øvrebø KM, Mathiesen B, and Rofstad EK (2011). Differentiation between hypoxic and non-hypoxic experimental tumors by dynamic contrast-enhanced magnetic resonance imaging. *Radiother Oncol* **98**, 360–364.

[29] Egeland TAM, Gulliksrud K, Gaustad JV, Mathiesen B, and Rofstad EK (2012). Dynamic contrast-enhanced MRI of tumor hypoxia. *Magn Reson Med* **67**, 519–530.

[30] Hittmair K, Gomiscek G, Langenberger K, Recht M, Imhof H, and Kramer J (1994). Method for the quantitative assessment of contrast agent uptake in dynamic contrast-enhanced MRI. *Magn Reson Med* **31**, 567–571.

[31] Benjaminsen IC, Graff BA, Brurberg KG, and Rofstad EK (2004). Assessment of tumor blood perfusion by high-resolution dynamic contrast-enhanced MRI: a preclinical study of human melanoma xenografts. *Magn Reson Med* **52**, 269–276.

[32] Tofts PS, Brix G, Buckley DL, Evelhoch JL, Henderson E, Knopp MV, Larsson HBW, Lee T-Y, Mayr NA, Parker GJM, et al. (1999). Estimating kinetic parameters from dynamic contrast-enhanced T_1-weighted MRI of a diffusable tracer: standardized quantities and symbols. *J Magn Reson Imaging* **10**, 223–232.

[33] Ozerdem U and Hargens AR (2005). A simple method for measuring interstitial fluid pressure in cancer tissues. *Microvasc Res* **70**, 116–120.

[34] Rofstad EK and Måseide K (1999). Radiobiological and immunohistochemical assessment of hypoxia in human melanoma xenografts: acute and chronic hypoxia in individual tumours. *Int J Radiat Biol* **75**, 1377–1393.

[35] Rofstad EK, Galappathi K, Mathiesen B, and Ruud EBM (2007). Fluctuating and diffusion-limited hypoxia in hypoxia-induced metastasis. *Clin Cancer Res* **13**, 1971–1978.

[36] Walenta S, Schroeder T, and Mueller-Klieser W (2002). Metabolic mapping with bioluminescence: basic and clinical relevance. *Biomol Eng* **18**, 249–262.

[37] Walenta S, Schroeder T, and Mueller-Klieser W (2004). Lactate in solid malignant tumors: potential basis of a metabolic classification in clinical oncology. *Curr Med Chem* **11**, 2195–2204.

[38] Sattler UG, Walenta S, and Mueller-Klieser W (2007). A bioluminescence technique for quantitative and structure-associated imaging of pyruvate. *Lab Invest* **87**, 84–92.

[39] Mueller-Klieser W and Walenta S (1993). Geographical mapping of metabolites in biological tissue with quantitative bioluminescence and single photon imaging. *Histochem J* **25**, 407–420.

[40] DeBerardinis RJ, Mancuso A, Daikhin E, Nissim I, Yudkoff M, Wehrli S, and Thompson CB (2007). Beyond aerobic glycolysis: transformed cells can engage in glutamine metabolism that exceeds the requirement for protein and nucleotide synthesis. *Proc Natl Acad Sci USA* **104**, 19345–19350.

[41] Vaupel P, Kallinowski F, and Okunieff P (1989). Blood flow, oxygen and nutrient supply, and metabolic microenvironment of human tumors: a review. *Cancer Res* **49**, 6449–6465.

[42] Gulledge CJ and Dewhirst MW (1996). Tumor oxygenation: a matter of supply and demand. *Anticancer Res* **16**, 741–750.

[43] Gatenby RA and Gillies RJ (2004). Why do cancers have high aerobic glycolysis? *Nat Rev Cancer* **4**, 891–899.

[44] Ellingsen C, Øvrebø KM, Galappathi K, Mathiesen B, and Rofstad EK (2012). pO_2 fluctuation pattern and cycling hypoxia in human cervical carcinoma and melanoma xenografts. *Int J Radiat Oncol Biol Phys* **83**, 1317–1323.

[45] Kroeger M, Walenta S, Rofstad EK, and Mueller-Klieser W (1995). Growth rates or radiobiological hypoxia are not correlated with local metabolite content in human melanoma xenografts with similar vascular network. *Br J Cancer* **72**, 912–916.

[46] Walenta S, Snyder S, Haroon ZA, Braun RD, Amin K, Brizel D, Mueller-Klieser W, Chance B, and Dewhirst MW (2001). Tissue gradients of energy metabolites mirror oxygen tension gradients in a rat mammary carcinoma model. *Int J Radiat Oncol Biol Phys* **51**, 840–848.

[47] Schroeder T, Yuan H, Viglianti BL, Peltz C, Asopa S, Vujaskovic Z, and Dewhirst MW (2005). Spatial heterogeneity and oxygen dependence of glucose consumption in R3230Ac and fibrosarcomas of the Fischer 344 rat. *Cancer Res* **65**, 5163–5171.

[48] Yaromina A, Quennet V, Zips D, Meyer S, Shakirin G, Walenta S, Mueller-Klieser W, and Baumann M (2009). Co-localisation of hypoxia and perfusion markers with parameters of glucose metabolism in human squamous cell carcinoma (hSCC) xenografts. *Int J Radiat Biol* **85**, 972–980.

[49] Walenta S and Mueller-Klieser W (2004). Lactate: mirror and motor of tumor malignancy. *Semin Radiat Oncol* **14**, 267–274.

[50] Busk M, Horsman MR, Kristjansen PEG, van der Kogel AJ, Bussink J, and Overgaard J (2008). Aerobic glycolysis in cancers: implications for the usability of oxygen-responsive genes and fluorodeoxyglucose-PET as markers of tissue hypoxia. *Int J Cancer* **122**, 2726–2734.

[51] Rofstad EK (2000). Microenvironment-induced cancer metastasis. *Int J Radiat Biol* **76**, 589–605.

[52] Lunt SJ, Chaudary N, and Hill RP (2009). The tumor microenvironment and metastatic disease. *Clin Exp Metastasis* **26**, 19–34.

[53] Chan DA and Giaccia A (2007). Hypoxia, gene expression, and metastasis. *Cancer Metastasis Rev* **26**, 333–339.

[54] Hirschhaeuser F, Sattler UGA, and Mueller-Klieser W (2011). Lactate: a metabolic key player in cancer. *Cancer Res* **71**, 6921–6925.

[55] Rutkowski JM and Swartz MA (2007). A driving force for change: interstitial flow as a morphoregulator. *Trends Cell Biol* **17**, 44–50.

[56] Mumprecht V and Detmar M (2009). Lymphangiogenesis and cancer metastasis. *J Cell Mol Med* **13**, 1405–1416.

[57] Hompland T, Ellingsen C, Galappathi K, and Rofstad EK (2013). Connective tissue of cervical carcinoma xenografts: associations with tumor hypoxia and interstitial fluid pressure and its assessment by DCE-MRI and DW-MRI. *Acta Oncol*, Epub ahead of print February 27.

[58] Hallac RR, Ding Y, Yuan Q, McColl RW, Lea J, Sims RD, Weatherall PT, and Mason RP (2012). Oxygenation in cervical cancer and normal uterine cervix assessed using blood oxygenation level-dependent (BOLD) MRI at 3T. *NMR Biomed* **25**, 1321–1330.

[59] Hompland T, Ellingsen C, Øvrebø KM, and Rofstad EK (2012). Interstitial fluid pressure and associated lymph node metastasis revealed in tumors by dynamic contrast-enhanced MRI. *Cancer Res* **72**, 4899–4908.

[60] Serganova I, Rizwan A, Ni X, Thakur SB, Vider J, Russell J, Blasberg R, and Koutcher JA (2011). Metabolic imaging: a link between lactate dehydrogenase A, lactate, and tumor phenotype. *Clin Cancer Res* **17**, 6250–6261.